How Complementary are SRTM-X and -C Band Digital Elevation Models?

Jörn Hoffmann and Diana Walter

Abstract

Two different digital elevation models (DEM) were derived during the 2000 Shuttle Radar Topography Mission from C- and X-band interferometric radar data. While these two DEMs share several of their properties, they were processed independently. Here, we investigate what can be gained by merging the two DEMs into a single composite DEM for four different test areas. Based on an analysis of the relative differences and the deviations from an absolute reference in one test area, we propose an algorithm for combining the two DEMs optimally. We then compare the composite DEM with both individual DEMs and with a reference of a large number of precise GPS profiles in one test area in southern Germany. We find that in our test areas, the area of missing values is reduced significantly in the composite DEM. Even compared with the more complete C-band DEM, the number of void pixels can be reduced by 22 percent to 53 percent. Also, outlier values resulting from errors in the interferometric phase unwrapping can often be identified and removed in the merging. The deviations of both C- and X-band DEMs from the GPS reference are very similar and well within the accuracy specifications of the global data set. The standard deviation of the difference between the composite DEM and the reference is about 14 percent below that of the original values. Depending on the requirements for completeness and accuracy, merging the two SRTM elevation data sets may provide an important improvement above either of the original DEMs.

Introduction

The main objective of the Shuttle Radar Topography Mission (SRTM) was to obtain a near-global digital elevation model (DEM) with a globally uniform high-resolution and quality. The SRTM was conducted in cooperation between the National Aeronautics and Space Administration (NASA), the German Aerospace Center (DLR), the Italian Space Agency (ASI), and the National Geospatial Intelligence Agency (NGA).

Interferometric Synthetic Aperture Radar (INSAR) data was acquired from 11 to 22 February 2000 by two radar systems mounted on the space shuttle. Each radar system consisted of two separate radar antennas, one in the shuttle cargo bay and the other one at the end of a 60 m beam (Rabus *et al.*, 2003). The Jet Propulsion Laboratory (JPL) of NASA operated a C-band system in ScanSAR mode covering a 225 km swath, and thus providing an almost complete DEM in the 56°S to 60°N latitude range. The DLR operated an X-band system with a swath width of 50 km. The much more limited swath width did not allow the acquisition of global data during the 10-day mission. Given similar signal to noise ratios and the same platform, interferometric baseline, and viewing geometry, the random error for a single observation at X-band is about one-half of that at C-band. This expectation is reflected in the slightly lower relative vertical error specified for the X-band DEM (Table 1). Note that these specifications reflect pre-mission requirements. Due to the greater swath width of the C-band instrument several observations were available for most locations, balancing this advantage of the X-band instrument to some extent.

The C- and X-band data sets were processed independently into two separate DEMs at JPL and DLR, respectively. The 1″ C-band DEM is publicly available only for the United States, and a reduced 3″ DEM was created and is publicly available globally (USGS, 2005b). The NGA post-processed the C-band DEM created by JPL and is responsible for the limited distribution of the full resolution 1″ C-band DEM. This complete data set includes not only the elevation data itself, but also an Orthorectified Image Mosaic (OIM) from the radar amplitude data, the Terrain Height Error Data (THED) derived during the interferometric processing, and a Seam Hole Composite Map (SHCM) showing location of image seams from the original acquisitions and data voids in the data. The data distributed openly only includes the elevation values, but not the OIM, THED, or SHCM.

The X-band DEM is available from DLR and its commercial distributors. The standard distribution includes the elevation data and the Height Error Map (HEM).

In processing the data acquired at the two radar frequencies separately, an opportunity was missed to exploit the advantages of each frequency in obtaining the best possible DEM from the mission. A simultaneous processing of both data sets would, among other advantages, have provided the rare opportunity of determining the integer phase ambiguity during interferometric phase unwrapping relatively robustly.

However, since the raw interferometric data from the mission is not available, and a reprocessing of the data certainly prohibitive in scope, our objective here was to investigate how the two final output products, i.e., the C- and X-band DEM, may be merged optimally and what can be gained by doing so.

This investigation was commissioned by the Geoinformation Office of the German Federal Armed Forces (AGEOBW), who provided us with the full resolution (1″) C-band DEM and the corresponding THED and SHCM data for four test regions. These were the object of a cooperative data swap between NGA and AGEOBW.

German Aerospace Center, German Remote Sensing Data Center, Postfach 1116, 82234 Wessling, Germany (joern.hoffmann@dlr.de).

Photogrammetric Engineering & Remote Sensing
Vol. 72, No. 3, March 2006, pp. 261–268.

0099-1112/06/7203–0261/$3.00/0
© 2006 American Society for Photogrammetry and Remote Sensing

TABLE 1. SPECIFICATIONS OF GLOBAL SRTM DEMS [USGS, 2005A; WAGNER, 2003]. ACCURACIES SPECIFIED ARE 90 PERCENT VERTICAL AND CIRCULAR ERROR LEVELS FOR VERTICAL AND HORIZONTAL ACCURACIES, RESPECTIVELY

Parameter	C-band	X-band
System		
Wavelength	5.6 cm	3.1 cm
Carrier frequency	5.3 GHz	9.6 GHz
Polarization	dual	VV
Swath width	225 km	50 km
Product		
Relative vertical accuracy	10 m	6 m
Absolute vertical accuracy	16 m	16 m
Relative horizontal accuracy	15 m	15 m
Absolute horizontal accuracy	20 m	20 m
Elevation steps	1 m	1 m
Grid postings	1″	1″
Vertical datum	EGM96	WGS84
Horizontal datum	WGS84	WGS84

We compared these data with the X-band DEM for the same areas and analyzed their differences and complementariness. For one test area in southern Germany, we also used GPS profiles as an absolute reference to assess the qualities of the two DEMs.

Data

We selected four diverse test regions in which we analyzed the differences between the DEMs derived from the C- and X-band SRTM data (Figure 1, Table 2). The test regions were selected on different continents and represent very different topographic regimes and land-cover types. Test Area 1 covers the south of Germany and northern parts of Switzerland and Austria. The elevations range from 212 m to over 3,700 m in the Alps. The climate is temperate, and much of the land surface at lower elevations is forested or farmed.

Test Area 2 is located in the remote eastern part of Afghanistan and includes part of Pakistan. The topography is very rugged and elevations range from 550 m to almost 7,000 m at the peaks. The climate is relatively dry, and much of the land surface is barren.

Test Area 3 is a sandy desert area in Mauritania with little topographic relief. Elevations are between 271 m and 537 m. The climate is extremely dry, and the land surface primarily consists of bare sand with extensive dunes.

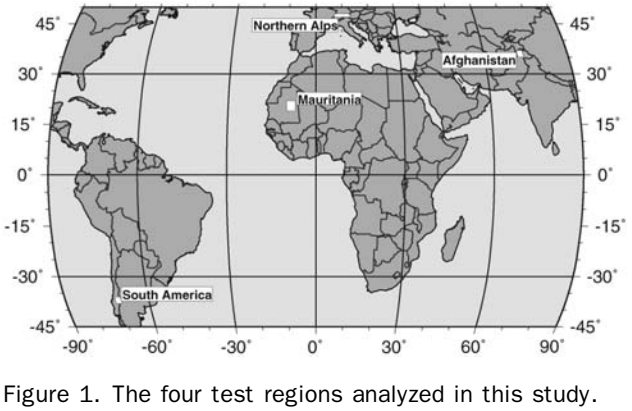

Figure 1. The four test regions analyzed in this study. See Table 2 for details.

TABLE 2. GEOGRAPHIC EXTENT OF THE FOUR TEST REGIONS INVESTIGATED IN THIS STUDY. (ALSO SEE FIGURE 1.)

	test area	North-west Corner		South-east Corner	
1	Northern Alps	48°N	7°E	47°N	13°E
2	Afghanistan	37°N	72°E	35°N	74°E
3	Mauritania	22°N	10°W	19°N	7°W
4	South America	36°S	72°W	38°S	70°W

Test Area 4 is located in the southward extension of the Andes on the border between Chile and Argentina. The relief is mostly relatively gentle with rolling terrain and elevations ranging from 147 m to 4,724 m.

Two data sets were analyzed and compared in these four test areas. The first was the 1″ DEM derived from the SRTM-C band data by JPL and post-edited by NGA. In particular, the post-editing performed by NGA included the editing of significant water bodies and the filling of small regions of invalids. The data were originally referenced to the EGM96 geoid. We corrected the values for the elevations of the geoid to compare them directly to the X-band DEM. The C-band data set available to us also included the Terrain Height Error Data (THED), which provides an error estimate for the 90 percent error level for each elevation (SRTM DPS, 2001).

The second data set was the DEM derived from the SRTM-X band data by DLR (Rabus *et al.*, 2003). This data is also at 1″ postings, but has not been post-processed systematically, e.g., to mask water bodies, identify individual outlier values, or smooth the elevation values. The elevations are referenced to the WGS84 ellipsoid. The X-band data set also included a Height Error Map (HEM), providing a standard error (1 σ) estimate for each elevation value (Knöpfle *et al.*, 1998).

Comparison of C- and X-band DEMs

The SAR antennas acquiring C- and X-band data during the SRTM mission realized almost identical geometries and were operated simultaneously. However, the processing into DEMs was done separately for the two data sets at different institutions using different processors. As mentioned before, the specifications for the two resulting DEMs were also slightly different (Table 1).

We analyzed the two DEMs in our four test regions with respect to their appearance, horizontal positioning, completeness, and complementariness. First, we subtracted the EGM96 elevations from the C-band DEM so that both DEMs were referenced to the WGS84 ellipsoid.

Given the common mission design it is not surprising that the two DEMs resulting from the SRTM mission look very similar. Of course, an obvious difference is the more limited coverage of the X-band DEM due to the much narrower image swath. A comparison of color-shaded reliefs of the two DEMs (Plate 1) shows a much noisier appearance of the X-band DEM. This is also apparent in spectrums of the spatial frequencies of the two images (Figure 2), which highlights that no post-editing has been performed on the X-band DEM. On the other hand, the high-frequency contributions appear to have been attenuated during processing of the C-band data. The post-editing is particularly obvious on the lake surface visible on the left of Plate 1, where the low signal-to-noise (SNR) results in a very high elevation noise level in the X-band DEM, while post-editing in the C-band DEM has removed a similar effect. It is important to point out that this noise represents pixel-to-pixel random noise in the data set and does not compromise the absolute accuracy of the

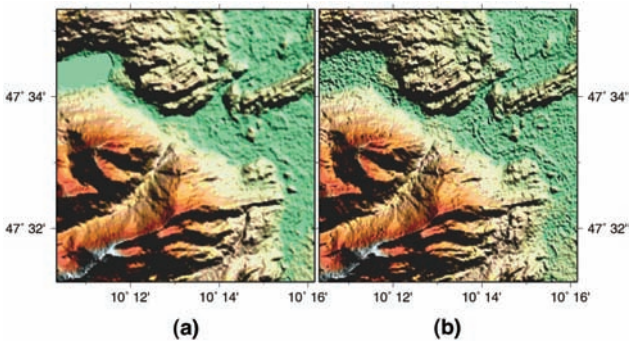

Plate 1. Comparison of the color-coded shaded relief view of the C-band (a) and X-band (b) DEMs. The higher level of elevation noise in the unedited X-band DEM is accentuated by the shaded-relief view, but retains some details strongly attenuated in the C-band DEM.

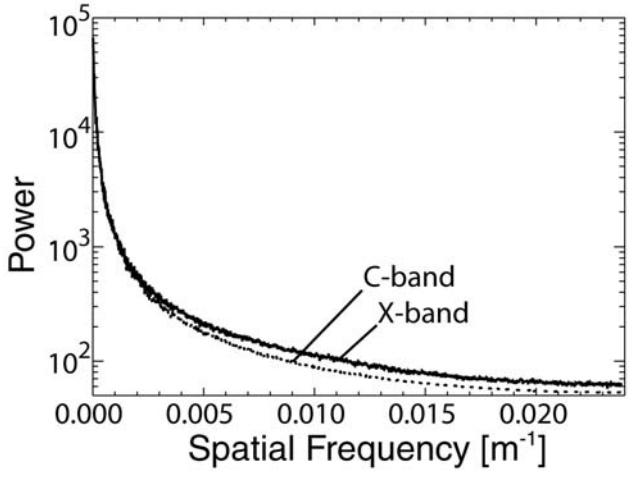

Figure 2. Spectrums of spatial frequencies for the area shown in Plate 1 for the two DEMs. The higher level of elevation noise in the X-band DEM appears as a greater high-frequency content in the spectrum.

DEM. Furthermore, the shaded-relief view accentuates this noise so that the X-band DEM may appear less accurate than the C-band DEM. The higher level of smoothness enforced for the C-band DEM, however, comes at the price of a loss in detail. This is visible, for example, at the center right of the area shown in Plate 1. The elevated river banks of the river Iller are clearly visible in the X-band DEM, but far less so in the C-band DEM. Finally, the impression that the C-band DEM is more accurate than the X-band DEM is not supported by our detailed comparison of the two DEMs to an absolute reference.

The comparison and merging of the two DEM data sets described below is performed on a pixel-by-pixel basis. It is therefore critical to ensure that these two data sets are aligned correctly. To test the data for any differences in horizontal position, we computed local cross-correlations on square regions at a large number of positions. We selected positions on a regular grid of 19 by 19 nodes for each 1 degree by 1 degree region in each of the four test areas. Where at least 50 percent of the pixels in both DEMs contained valid points, we computed the peak of the cross-correlation function of a 64 pixel by 64 pixel region centered on the position, over-sampled by a factor of 2. Unfortunately, the radar amplitude image derived from the C-band data (OIM (SRTM DPS, 2001)) was not available to us. The procedure would probably have been much more effective using the amplitude data instead of the elevation data. In some instances the peak of the cross-correlation was poorly constrained, particularly in places of little topographic relief or on large water bodies. However, in the vast majority of locations the peak of the cross-correlation function was exactly at zero offset. Importantly, we detected no systematic horizontal offset between the two DEMs in any of our test areas.

However, in some areas we observe a significant vertical offset between the C- and X-band DEMs. This is negligible in our alpine test area, but for the South America test area the C-band values are about 10 m higher than the X-band values. A global map of this difference (Plate 2) derived from the X-band DEM and the 3″ C-band DEM distributed by the United States Geological Survey (USGS, 2005b) shows that the offsets are spatially highly correlated and vary slowly in space. The largest differences occur as a systematic bias of low spatial frequencies and are particularly pronounced in Africa and South America (see yellow and green areas in Plate 2). These probably result from differences in the block adjustment of the DEMs.

By design, the SRTM mission acquired interferometric data for the derivation of DEMs over land surface areas between 56°S and 60°N. Due to the greater width of the swath imaged at C-band, the C-band DEM covers about 80 percent (approximately 120 million km^2) (JPL, 2005) of the land surface between these latitudes, while the X-band covers only 40 percent (approximately 58 million km^2) (Roth *et al.*, 2001). Consequently, the X-band DEM is only available on a mesh with holes of increasing size towards lower latitudes. The fraction of missing values due to the limited coverage in our test areas ranges from 34 percent in the Alps to 67 percent in the Mauritania test areas (Table 3).

The area without data acquisitions during the mission is much smaller at C-band. Nevertheless, the final DEM contains invalids in regions where no reliable elevation value could be derived during the processing. Mostly these void regions relate to difficulties in the phase unwrapping in rugged mountainous terrain. In our test areas between

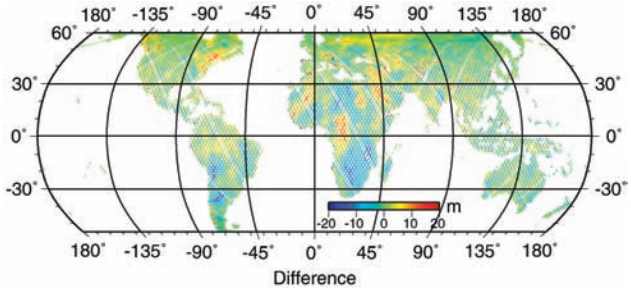

Plate 2. The large-scale differences between the two SRTM DEMs. A spatially slowly varying offset between the C- and X-band DEMs is observed when comparing the DEMs at these larger scales (note the green and yellow areas).

TABLE 3. COMPLETENESS OF DEMS DERIVED FROM SRTM C- AND X-BAND DATA. THE INVALIDS IN THE X-BAND DEM ARE ONLY CONSIDERED IN REGIONS FOR WHICH DATA WAS ACQUIRED

Test Site	Invalids C-band	Invalids X-band	No Acquisition X-band	Holes Fillable in C-band	Invalid in C-and X-band
1	2.3%	0.0%	34.3%	52.7%	1.1%
2	20.4%	6.0%	59.4%	22.2%	16.0%
3	40.1%	0.0%	66.8%	29.3%	29.8%
4	0.3%	0.0%	44.4%	36.7%	0.1%

0.3 percent and 40.1 percent of the area was voided (Table 3). Over the entire data set the percentage of missing values in the C-band DEM is much closer to the former value, as we selected our test regions in regions where we expected the interferometric DEM generation to be difficult. For example, Hall *et al.* (2005) found 0.3 percent data voids in a sample of data over the United States.

The X-band DEM contains much fewer missing data within the data acquisitions. In contrast to the phase unwrapping algorithm used in the C-band processing the algorithm used for the X-band yielded a value at every location. Of course, difficulties of interferometric phase unwrapping generally occur in the same terrains for the two frequencies. In creating the C-band DEM, multiple data acquisitions were available at many locations to identify errors in the phase unwrapping. The X-band data covered much less area multiple times. Therefore, the DEM derivation could usually not draw on several observations for identifying such errors. Data voids in the X-band DEM were only introduced in a manual quality control after DEM generation in regions where the phase unwrapping had obviously failed. Less apparent errors affecting smaller regions were difficult to identify during the DEM generation and are still contained in the DEM. In our test areas only the Afghanistan test area had data voids within the acquisition swaths (Table 3).

Unfortunately, X-band voids often occur in regions where the C-band DEM does not provide a valid value either. This is not surprising, as these voids derive from difficulties in the interferometric processing for certain acquisition geometries. Nevertheless, the DEMs were derived independently from two separate data sets and the missing data regions are not completely congruent.

An interesting case in this context is the Mauritania test area. Here the data voids are not caused by the well-known difficulties of phase unwrapping in rugged terrain, but likely derive from low signal-to-noise ratio (SNR) and, consequently, high phase noise due to volume scattering in the very dry sand surface. The radar signal penetrates into the sand surface and is attenuated. As the penetration depth increases with increasing radar wavelength (Curlander and McDonough, 1991), this affects the C-band radar more than the X-band radar. Despite the fact that only one third of the Mauritania test site was covered by the X-band data takes, the X-band DEM can be used to decrease the percentage of data voids in the C-band DEM from 40 percent to 30 percent. It should be noted though, that even at X-band the attenuation of the radar signal was severe and the elevation errors annotated in the HEM exceed the specifications for the global data set (Table 1).

Overall we found that combining the two DEMs could significantly decrease the area of missing data. Between 22 percent and 53 percent of the data voids in the C-band DEM could be filled with information from the X-band DEM in our test areas (Table 3), in all cases decreasing the percentage of missing data significantly.

Validation

The Geoinformation Office of the German Federal Armed Forces ("Amt für Geoinformationswesen der Bundeswehr," AGEOBW) provided us with 1,125 GPS profiles with over 200.000 individual measurements collected in part of the German test area (Plate 3). These allowed us to validate the SRTM DEMs with respect to an absolute height reference for this test area. Unfortunately, no reliable absolute reference was available to us for the three other test areas.

The absolute accuracy of the GPS measurements is on the meter-level. Some differences between this reference and the SRTM models are expected, of course, where the roads on which the GPS data was collected cross bridges or where dense forest dominates the land-cover adjacent to the roads.

We interpolated the elevation at the GPS points from both SRTM DEMs using a bilinear interpolation from the four nearest grid points and compared the elevations with the GPS-measured values.

First, we tested for any systematic bias in the data. The median difference between C/X-band DEM and GPS values were −73 cm (mean: −26 cm) and −55 cm (mean: −17 cm), respectively. Note that elevation values in both SRTM DEMs are only specified as integer meters (Table 1). The minimum and maximum differences were −52 m and 45 m for the C-band DEM, and −54 m and 168 m for the X-band DEM, respectively. Interestingly, the latter value of 168 m is almost exactly the height of ambiguity for the X-band interferometer.

For both DEMs, 90 percent of the values differed less than 5 m from the GPS values and thus, are well within the global specifications in Table 1. Determined from their absolute accuracy and error statistics (Figure 3) the two DEMs prove to be of very similar quality.

This result is particularly important in the context of the noisier appearance of the shaded relief maps (Plate 1) discussed above. Despite the comparatively higher level of pixel-to-pixel elevation noise in the X-band DEM, the C-band DEM is not more accurate. A detailed analysis along individ-

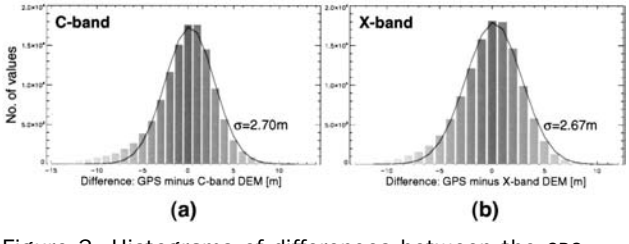

Figure 3. Histograms of differences between the GPS reference elevations and the SRTM C-band (a) and X-band (b) values. The error distributions are very similar and approximately follow a normal distribution. The effect of vegetation heights in the SRTM DEMs is apparent in the slightly more frequent negative values. Not visible at this scale is that larger differences are more common than expected for a normal distribution (see text). The standard deviations shown correspond to the overplotted curves. The sample standard deviations are 3.90 m and 3.99 m for C- and X-band, respectively.

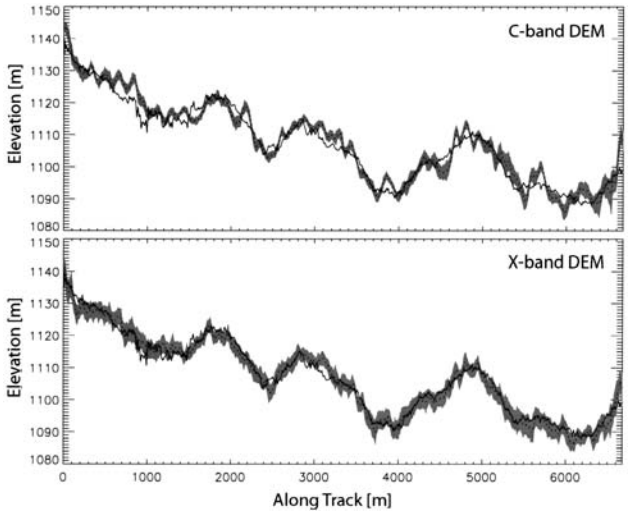

Figure 4. Comparison of C-and X-band DEMs with a GPS profile. The SRTM elevations are shown with 1 σ error bands from the THED or HEM. Note that the smoother C-band misses some small-scale detail shown in the GPS data. The X-band DEM contains more point-to-point scatter.

ual GPS profiles showed that in many instances the smoother C-band DEM misses true topographic variations, while the X-band DEM values scatter much more about the reference (Figure 4). On the other hand, the very similar quality of the two SRTM DEMs also shows that the advantages of a shorter radar wavelength to derive a higher-accuracy DEM seem to be balanced by the advantages of being able to draw on several observations due to the multiple observations (three for this location (JPL, 2005)) at the longer wavelength.

Another important observation is that the histograms of the differences between SRTM DEMs and the GPS reference (Figure 3) closely follow a normal distribution. However, there is a slight bias towards negative values, i.e., the elevation value in the SRTM DEMs is more often greater than the GPS value than the other way round. This can be explained with the difference between the surface model provided by the SRTM measurements and the ground elevations measured by the GPS survey.

Notwithstanding this observation, it must be emphasized that the SRTM errors are *not* normally distributed. Despite the appearance of the histograms in Figure 3, large differences (outliers) occur much more frequently than they should for normally distributed errors. These outlier values are probably related to unwrapping errors and thus occur much more frequently in areas of steep slopes (Falorni *et al.*, 2005). In our test areas, outlier values are more common in the X-band DEM. This can be explained with the fact that only single and dual coverages were available in the X-band acquisitions, severely limiting the opportunities of identifying outlier values during processing. Also, the height of ambiguity, i.e., the elevation difference corresponding to one ambiguity cycle in the interferometric phase difference, is proportional to the radar wavelength (Hanssen, 2001), and therefore much smaller for X-band acquisitions, further complicating the unwrapping procedure.

These observations were also confirmed by a relative comparison of the two SRTM DEMs in the other test areas. The differences between the C- and X-band DEM followed a Gaussian distribution, except for the fact that large differences (both positive and negative) were overly common.

Discussion

Our observations on the error distributions of the two SRTM DEMs suggest that the errors in the SRTM DEMs are largely normally distributed, with two important deviations from the Gaussian statistics:

1. There is a bias towards higher elevations in the SRTM DEMs due to the presence of vegetation when compared to a bare-earth reference.
2. Outlier values, likely caused by phase unwrapping errors during interferometric processing, occur more frequently than Gaussian statistics would predict. These outlier values are more common in the X-band DEM.

The former deviation from Gaussian statistics is of no particular concern for a relative comparison of the two DEMs. Although the C-band radar signal might penetrate slightly deeper into a vegetation layer and thus yield slightly lower elevation values in a DEM, the difference in penetration into canopy between C- and X-band is expected to be small.

The second point is more relevant, because an adequate error representation for both DEMs is critical to merging the DEMs optimally. The error maps, THED and HEM for C-band and X-band, respectively, only provide a relative error for a normally distributed statistical error. These errors essentially represent an elevation error propagated from the interferometric coherence value at that location (Knöpfle *et al.*, 1998). While these error estimates already quantify the effects of many error contributions like acquisition geometry, signal noise, or reduced interferometric coherence, they cannot adequately account for unwrapping errors resulting in significant height errors in the final DEM. Undetected unwrapping errors will usually coincide with regions of reduced interferometric coherence and, consequently, higher error levels, but the assumption of Gaussian statistics intrinsic to the error propagation and representation is not applicable.

We therefore conceptualize the total relative error of the SRTM DEMs as the sum of two components, namely:

1. A normally distributed statistical error due to a number of error contributions and described by the THED or HEM error estimates, and
2. An "outlier component" due to undetected errors in the phase unwrapping.

This conceptualization can aide the adequate quantification of errors in the DEMs. Many tools and techniques exist to work with normally distributed errors. However, the deviations from the normal distribution of errors should generally be considered before we can draw on these.

The most direct way to do this is to identify outlier values in the elevation dataset. They can then be removed or an attempt to correct the elevation value based on neighborhood information can be made. At least the outliers should be flagged. Unfortunately, it is difficult to detect outlier values reliably without extensive independent elevation information. Of course, dramatic outliers, deviating several hundred meters from the surrounding elevation pixels are easily identified. But outliers caused by unwrapping errors are affected additionally by phase noise and the effects of the interpolation during the gridding, so that the deviations are not always extremely pronounced.

Also, where not only individual pixels are affected, but large regions in the DEMs are offset from the true elevations, a relative comparison to the neighborhood elevations cannot be used to identify the error.

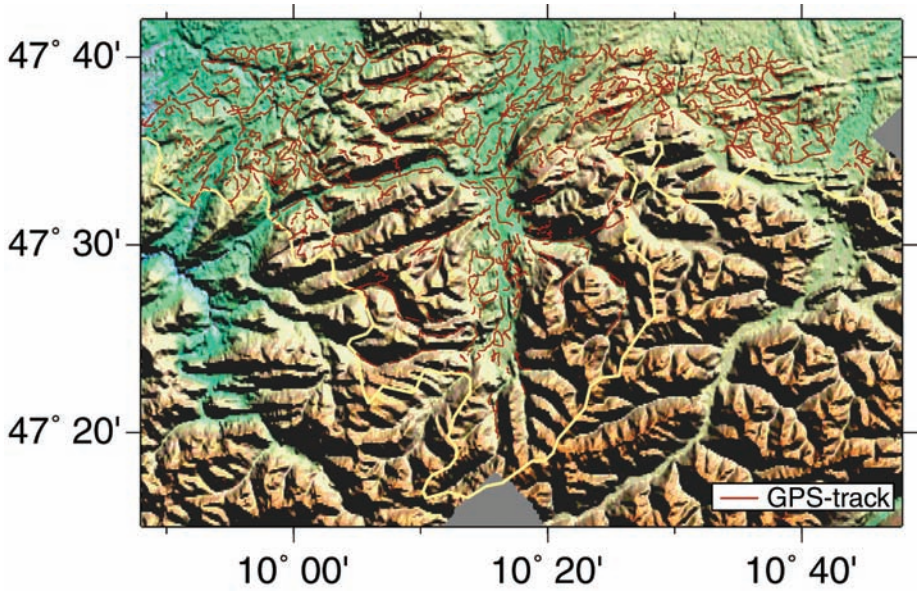

Plate 3. Map view of available GPS profiles used as absolute reference for validation of the SRTM DEMs.

The following section will detail an approach that considers some of these difficulties and tries to merge the two SRTM DEMs in an optimal fashion.

Combining C- and X-band DEMs

Ideally the data acquired at the two radar frequencies during the SRTM mission should have been processed into a single DEM from the start. This would have resulted in a superior final result, as more observations would have reduced the random error and, more importantly, combining two frequencies would have greatly aided the phase unwrapping. Resolving the integer ambiguities during phase unwrapping would have been significantly more robust, even in challenging situations, had the two wrapped interferograms been used.

Our objective here was to investigate how much the two separate DEMs that have been created from SRTM data can profit from a combination of the final products. Primarily, improvements are expected in a reduction of areas lacking observations (i.e., voids), a decreasing statistical error, and an identification of outlier values. The characteristics of the accuracies and elevation error statistics discussed in the previous sections suggest that existing tools for Gaussian error distributions can be used for merging the DEMs, provided that the presence of outliers from unwrapping errors and low-frequency large offsets are accounted for separately. We thus propose the following algorithm, which is based on the mosaicking algorithm described by Knöpfle *et al.* (1998). The algorithm constitutes a least-squares optimal combination of different elevation values with normally distributed errors and separate considerations of low-frequency vertical offsets and individual outlier values.

The following steps are performed:

1. Masking water bodies in X-band DEM.
2. Detecting outliers in individual DEMs based on local statistics.
3. Removing low-frequency vertical offset of DEMs using reference data where available.
4. Detecting outliers by thresholding the difference between C- and X-band DEM.
5. Variance-weighted averaging of elevation values, including error propagation.

Ideally, if independent information on water bodies is available from reliable sources, this can be used. Otherwise it may to some extent be possible to extract these areas from the C-band DEM, which has already been edited using such information. Fortunately, we were able to use the THED to identify water regions in our test areas and mask them in the X-band data. The THED has a value of zero in areas where water bodies have been derived from independent information during editing (SRTM DPS, 2001). In the absence of adequate independent information on the location and extent of water bodies this masking step can be difficult and very time-consuming. Fortunately though, substantial effort has already been expended to define an SRTM water body product, and the SRTM Water Body Data (SWBD) is publicly available.

The outlier detection based on local statistics (Step Number 2 above) is important primarily for the X-band DEM, which has profited much less from multiple coverages in identifying outliers. For our test regions we thresholded the deviation from the median elevation value in a square area of five pixels width centered on each pixel. If the local median differed by over 100 m from the center pixel elevation and was outside the 95 percent confidence interval of the center pixel elevation based on Gaussian statistics and the error estimate from HEM or THED, we removed the center pixel from the DEM. We did not attempt to optimize these threshold values systematically. In general the threshold should probably be adjusted to the terrain type.

Systematic errors in the SRTM DEMs cause spatially low-frequency deviations between the two DEMs (Plate 2). These should be determined and corrected prior to a pixel-by-pixel averaging of the elevation values. Ideally this should be done using independent elevation information at reference points. These need not be available at high spatial detail to constrain the low frequency correction. Even a single reference elevation per 1° square area may be sufficient. Where no reliable independent information is available, the relative offset should still be removed prior to averaging. For

our test areas for which we did not have reference information we used the C-band DEM as a reference.

A second attempt is made to identify outlier values based on the difference between the two DEMs where both DEMs provide valid elevation values (Step Number 4 above). An outlier value is flagged where the difference between X- and C-band falls outside the 95 percent confidence interval (based on Gauss statistics and the error estimate from HEM or THED) and exceeds a predefined threshold of 50 m. Again, the threshold value should depend on the local terrain type. As discussed above, we anticipate undetected unwrapping errors to be more common in the X-band DEM. Therefore, where outliers were detected based on this criterion we removed the X-band elevation value from the DEM.

Finally (Step Number 5), an error-variance weighted average is computed based on the error estimates in the HEM and THED layers. The merged elevation estimate is computed as

$$h = \frac{\tilde{\sigma}_c^{-2} h_x + \tilde{\sigma}_x^{-2} h_c}{\tilde{\sigma}_c^{-2} + \tilde{\sigma}_x^{-2}}. \quad (1)$$

Here h_c and h_x are the elevations in the C- and X-band DEMs, respectively, after Steps 1 through 4 above. The variances $\tilde{\sigma}_c^2$ and $\tilde{\sigma}_x^2$ are the values derived from the error estimates in the THED and HEM layers, respectively, plus an additional error that is introduced to transition smoothly at the boundaries of invalid regions, $\Delta\sigma_c^2$ and $\Delta\sigma_x^2$ (Knöpfle *et al.*, 1998):

$$\tilde{\sigma}_c^2 = \sigma_c^2 + \Delta\sigma_c^2$$
$$\tilde{\sigma}_x^2 = \sigma_x^2 + \Delta\sigma_x^2.$$

The error variance of the estimate h is then computed as

$$\sigma^2 = \frac{\tilde{\sigma}_c^{-2}\sigma_x^2 + \tilde{\sigma}_x^{-2}\sigma_c^2}{\tilde{\sigma}_c^{-2} + \tilde{\sigma}_x^{-2}}. \quad (2)$$

Results

We applied the algorithm described in the previous section to the data in our test areas. Visual inspection of the color shaded relief images confirms that the resulting DEM combines properties of both input data sets. The result is smoother than the X-band DEM and more structured than the C-band DEM (Plate 4).

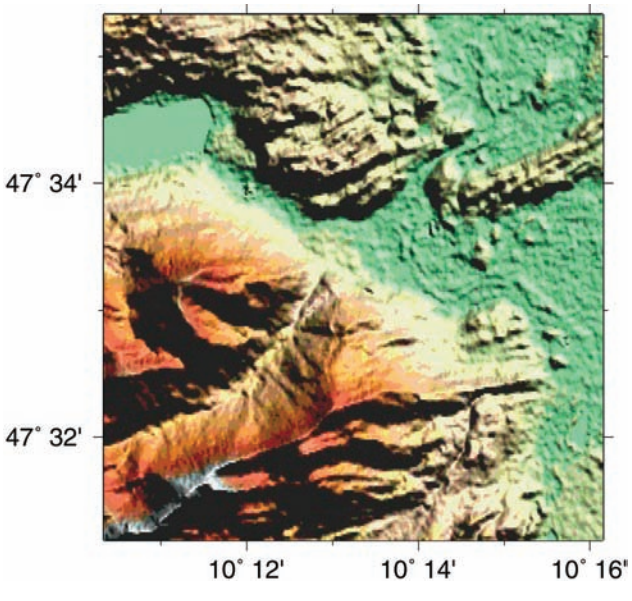

Plate 4. Color-coded shaded relief view of merging result for the area shown in Plate 1.

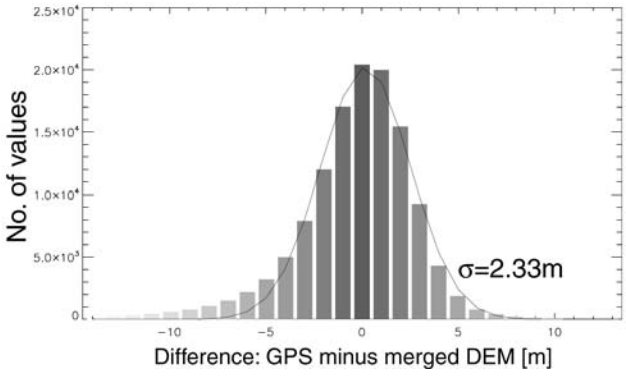

Figure 5. Histogram of differences between the GPS reference elevations and the composite DEM. The error distribution is characterized by a smaller standard deviation than either distribution for the input DEMs. Note that the standard deviation specified in the plot corresponds to the overlaid Gauss curve. The standard deviation of the histogram sample is 3.4 m.

The histogram of the deviations from the GPS reference data (Figure 5) shows that the standard errors of the result have decreased by about 14 percent with respect to either individual DEM. Also, the number of outliers from unwrapping errors has decreased in comparison to the original X-band DEM.

As expected, combining the two DEMs has also improved the completeness as quantified in Table 3.

Conclusions

We have evaluated the benefit of merging the two DEMs derived from the C- and X-band data acquired during the SRTM mission for four test areas. Considering the error statistics of both SRTM DEMs, we have proposed an algorithm for combining the DEMs optimally, taking into account the error information provided for the elevation values.

We found that the resulting combined DEM is superior to either input DEM in two main respects, namely completeness and reduced random errors. For our four test areas the number of void values in the C-band DEM could be reduced by 22 percent to 53 percent. The standard deviation of the differences between the two SRTM DEM and an absolute elevation reference for our test area in southern Germany was decreased by about 14 percent from 3.9 m and 4.0 m for C- and X-band DEM, respectively, to 3.4 m.

Of course, the significance of the improvements varies dramatically for different regions, depending on the size of void areas and elevation accuracies of the input DEMS, but also on the accuracies required for the final DEM.

Acknowledgments

The work described in this paper was conducted in a project funded by the Geoinformation Office of the German Federal Armed Forces ("Amt für Geoinformationswesen der Bundeswehr," AGeoBw), who also provided the GPS reference data for the German test area.

References

Curlander, J.C., and R.N. McDonough, 1991. *Synthetic Aperture Radar*, Wiley Series in Remote Sensing, John Wiley.

Falorni, G., V. Teles, E.R. Vivoni, R.L. Bras, and K.S. Amaratunga, 2005. Analysis and characterization of the vertical accuracy of digital elevation models from the shuttle radar topography mission, *Journal of Geophysical Research*, 110, F02, 005.

Hall, O., G. Falorni, and R.L. Bras, 2005. Characterization and quantification of data voids in the shuttle radar topography mission data, *IEEE Geoscience and Remote Sensing Letters*.

Hanssen, R.F., 2001 *Radar Interferometry – Data Interpretation and Error Analysis*, Kluwer Academic Publishers.

JPL, 2005. Shuttle radar topography mission – coverage, URL: http://www2.jpl.nasa.gov/srtm/coverage.html (last date accessed: 12 December 2005).

Knöpfle, W., G. Strunz, and A. Roth, 1998. Mosaicking of digital elevation models derived by SAR interferometry, *International Archives of Photogrammetry and Remote Sensing*, 32, pp. 306–313.

Rabus, B., M. Eineder, A. Roth, and R. Bamler, 2003. The shuttle radar topography mission (SRTM) – A new class of digital elevation models acquired by spaceborne radar, *ISPRS Journal of Photogrammetry and Remote Sensing*, 57, pp. 241–262, doi: 10.1016/S0924-2716(02)00124-7.

Roth, A., M. Eineder, B. Rabus, E. Mikusch, and B. Schättler, 2001. SRTM/XSAR: Products and processing facility, Proceedings of the *Geoscience and Remote Sensing Symposium, IGARSS '01*, Volume 2, pp. 745–747.

SRTM DPS, 2001. Shuttle Radar Topography Mission (SRTM) Data Products Specification, *Technical Report*, Version 1.3, National Imagery and Mapping Agency.

USGS, 2005a. Shuttle radar topography mission (SRTM) 1 arc second (30m), URL: http://seamless.usgs.gov/website/seamless/products/srtm1arc.asp (last date accessed: 12 December 2005).

USGS, 2005b. Shuttle radar topography mission, URL: http://srtm.usgs.gov (last date accessed: 12 December 2005).

Wagner, M., 2003. SRTM DTED format, *Product Description SRTM/PD03/11/03, Version 1.1*, Deutsches Zentrum für Luft- und Raumfahrt, 2003 URL: http://www.dlr.de/srtm/produkte/SRTM-XSAR-DEM-DTED-1.1. pdf (last date accessed: 12 December 2005).